ACS Medicinal Chemistry Letters

pubs.acs.org/acsmedchemlett Letter

Design and Synthesis of Fragment Derivatives with a Unique Inhibition Mechanism of the uPAR·uPA Interaction

Khuchtumur Bum-Erdene, Degang Liu, David Xu, Mona K. Ghozayel, and Samy O. Meroueh*

Cite This: *ACS Med. Chem. Lett.* 2021, 12, 60–66 Read Online

ACCESS | Metrics & More | Article Recommendations | Supporting Information

ABSTRACT: There is substantial interest in the development of small molecules that inhibit the tight and highly challenging protein−protein interaction between the glycophosphatidylinositol (GPI)-anchored cell surface receptor uPAR and the serine protease uPA. While preparing derivatives of a fragment-like compound that previously emerged from a computational screen, we identified compound **5** (IPR-3242), which inhibited binding of uPA to uPAR with submicromolar IC_{50}s. The high inhibition potency prompted us to carry out studies to rule out potential aggregation, lack of stability, reactivity, and nonspecific inhibition. We designed and prepared 16 derivatives to further explore the role of each substituent. Interestingly, the compounds only partially inhibited binding of a fluorescently labeled α-helical peptide that binds to uPAR at the uPAR·uPA interface. Collectively, the results suggest that the compounds bind to uPAR outside of the uPAR·uPA interface, trapping the receptor into a conformation that is not able to bind to uPA. Additional studies will have to be carried out to determine whether this unique inhibition mechanism can occur at the cell surface.

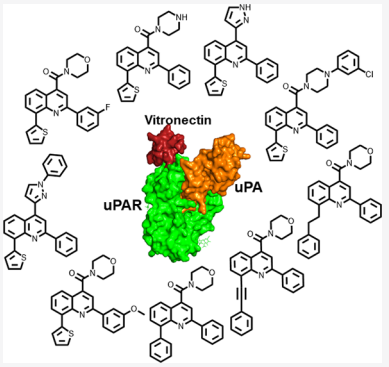

KEYWORDS: *uPAR, urokinase plasminogen activator receptor, protein−protein interaction, small-molecule inhibitor, fragment-based drug design*

Downloaded via UNIV OF CONNECTICUT on May 15, 2021 at 16:45:01 (UTC).
See https://pubs.acs.org/sharingguidelines for options on how to legitimately share published articles.

The urokinase plasminogen activator receptor (uPAR) is a glycophosphatidylinositol (GPI)-anchored receptor that serves as a docking site to the serine proteinase urokinase plasminogen activator (uPA)[1] and the somatomedin B (SMB) domain of the extracellular matrix glycoprotein vitronectin (VTN).[2−4] There is intense interest in developing antagonists of the uPAR·uPA interaction to explore the function of this interaction in a range of pathological processes such as inflammation, cancer, and cardiovascular disease. Most efforts to date have been confined to the use of biologics consisting of either fusion proteins[5−7] or peptides.[8−11]

uPAR binds to uPA with high affinity (K_D = 1 nM), and the complex is highly stable ($k_{off} = 10^{-4}$ s^{-1}).[12] X-ray structures of the uPAR·uPA complex reveal a large interaction interface (approximately 1500 $Å^2$) that contains a well-defined binding site.[13−16] The development of potent small-molecule inhibitors of this interaction remains a challenge, despite several attempts by us and others.[14,17−22] A structure-based design approach has been the main strategy to date. Small molecules are designed to bind in the deep hydrophobic pocket of uPAR, which accommodates the 25-residue β-hairpin from the uPA growth-factor-like domain (GFD). These strategies assume that uPAR adopts a similar structure in the apo and uPA-bound states, but there is evidence that uPAR is highly flexible and adopts a sheet-like structure in solution, which could explain the difficulty in developing potent small-molecule inhibitors.[23,24]

Previously, we reported the discovery of fragment **1** (IPR-2992), which binds to uPAR and inhibits its interaction with uPA.[25] The fragment revealed robust but weak inhibition of uPAR·uPA. To improve on its binding affinity and inhibition potency, we designed and synthesized several derivatives starting with the predicted binding mode of **1**. One of these derivatives, **5** (IPR-3242), exhibited unusually potent inhibition in our competition assays involving the entire uPAR·uPA protein−protein interface. To further explore the inhibition mechanism of the compounds, we prepared 16 derivatives and carried out extensive biochemical and biophysical studies to rule out potential aggregation and nonspecific effects.

Synthesis of Compound 1 Derivatives and Testing for Inhibition of uPAR·uPA_{ATF}. In previous work, we reported the discovery of fragment-like **1** (Figure 1).[25] To enhance the binding affinity and inhibition potency of the compound, we resorted to structure-based design using the predicted binding mode of **1** to uPAR.[25] We observed that the R_3 substituent (Table 1) pointed to a specific pocket on uPAR. Also, the R_3 group was not explored by similar compounds that we had previously identified from commercial sources. We designed and prepared compounds **2**−**6** by replacing the R_3 methyl

Received: July 31, 2020
Accepted: December 7, 2020
Published: December 10, 2020

© 2020 American Chemical Society

https://dx.doi.org/10.1021/acsmedchemlett.0c00422
ACS Med. Chem. Lett. 2021, 12, 60−66

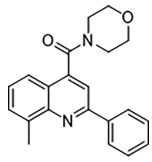

1 (IPR-2992)

Figure 1. Chemical structure of **1** (IPR-2992).

substituent of **1** with other larger groups (Table 1). These compounds were tested using a fluorescence polarization (FP) assay that uses a previously described fluorescently labeled α-helical peptide AE147 that binds to the uPA_{ATF} binding site (Figure 2A). We also tested the compounds using a microtiter-based enzyme-linked immunosorbent assay (ELISA), which, unlike the FP assay, includes the entire uPAR·uPA protein interface (Figure 2B). For the FP assay, two compounds, **5** and **6** (IPR-3243), revealed concentration-dependent inhibition, but the inhibition curves plateaued at about 40% (Figure 2A and Table 1). For the ELISA, two compounds exhibited complete inhibition of the uPAR·uPA interaction within the concentration ranges considered. Remarkably, compound **5** inhibited with submicromolar IC_{50} of 0.5 ± 0.0 μM (Table 1). The IC_{50} of **5** in this assay improved by 280-fold over the parent **1**, which was reported at 140.6 ± 19.0 μM.[25] Compound **5** did not interfere with the fluorescence of the AE147-FAM peptide (SI; Figure S1). Interestingly, replacing the thiophene of **5** with a phenyl moiety as in compound **2** (IPR-3238) resulted in substantially higher IC_{50} of 13.9 ± 1.5 μM. A phenylethyl group in **4** (IPR-3241) did not inhibit the interaction, and the phenylethynyl and isoindolinedione substituents in **3** (IPR-3239) and **6**, led to high double-digit IC_{50}s, 50.0 ± 6.0 μM and 73.8 ± 9.7 μM, respectively (Table 1). To confirm the ELISA results, we resorted to biolayer interferometry (BLI) in competition mode. Compound **5** inhibited the uPAR·uPA_{ATF} interaction in a concentration-dependent manner with an IC_{50} of 8.6 ± 0.2 μM (Figure 2C and D).

Biochemical Studies to Explore Potential Nonspecific Inhibition. The unusually high potency of **5**, especially considering its relatively low molecular weight and flat structure, prompted us to explore the possibility that the compound may be inhibiting through a nonspecific mechanism. First, the compound was tested for inhibition of other protein−protein interactions. Compound **5** was tested against two unrelated protein−protein interactions, namely, TEA Domain Transcription Factor 4 (TEAD4) and Yes-Associated protein 1 (Yap1), and voltage-gated calcium channel 2.2 beta subunit ($Cav2.2_{\beta 3}$) and the autoinhibitory domain (AID), for which we have established FP-based assays.[26,27] Both interactions are high-affinity protein−protein interactions with dissociation equilibrium constants in the nanomolar range, and they both occur over a large interface. The TEAD4·Yap1 interaction is devoid of a pocket and is considered a tertiary interaction as the interface involves multiple secondary structures of Yap1 binding to the surface of TEAD4. The $Cav2.2_{\beta 3}$·AID interaction is considered a secondary interaction as the interface consists of an α-helix (AID) binding to a pocket on the $Cav2.2_{\beta 3}$ subunit. The compounds did not inhibit either the binding of TEAD4 to Yap1 or $Cav2.2_{\beta 3}$ to the AID peptide (Figure 3A).

Next, we wanted to eliminate the possibility that the compound binds to uPA instead of uPAR to inhibit the protein−protein interaction. We used an ELISA similar to the one above except that uPA_{ATF} was placed on the microtiter plate. Compound **5** was incubated with surface-immobilized uPA_{ATF} for 30 min, and after several washing steps uPAR was added to the wells followed by detection to measure the extent of uPAR binding to immobilized uPA_{ATF}. The compound did not inhibit the protein−protein interaction, suggesting that **5** was unlikely inhibiting the protein−protein interaction by binding to uPA_{ATF} directly (Figure 3B).

Although our compounds do not seem to possess any moieties that are likely to react with nucleophiles on uPAR, we nevertheless used the fluorescence-based thiol-reactive assay (MSTI) to rule out covalent bond formation with cysteine. As expected, **5** and its derivatives did not react toward the activated nucleophile (Figure 3C). Next, we explored the possibility that the compound may inhibit through an aggregation mechanism. It is worth pointing out that the FP, ELISA or BLI curves do not suggest aggregation as an inhibition mechanism. The inhibition curves span two-log units of concentration. To rule out aggregation, we repeated the inhibition studies with increasing levels of detergent Triton X-100. Increased levels of detergent are known to disrupt aggregates. If the compounds inhibit through aggregation, then the activity of the compounds should be eliminated at higher detergent levels. However, increasing the levels of Triton X-100 in the ELISA assay from 0.01% to 0.1% did not affect the inhibition profile of **5** (Figure 3D). We also resorted to dynamic light scattering (DLS), another common approach to detect the presence of large particles. At higher concentrations of **5**, we did observe formation of large particles in assay buffer containing PBS and 0.01% Triton X-100. The aggregation was detectable at concentrations of 12.5 μM or higher (Figure 3E), with heterogeneous particle sizes being detected with diameters in the range of 150−2000 nm and high polydispersity (17−30%). The diameter and the polydispersity increased with increasing concentration of compound. The count rate also increases with increasing concentration of compound (Figure 3F). However, the concentration at which large particles are observed, 12.5 μM, is 25-fold higher than the IC_{50} of the compound in the ELISA assay. This along with the fact that a 10-fold increase in Triton X-100 levels showed no effect on compound activity suggests that aggregation is unlikely the mechanism by which the compound inhibits uPAR binding to uPA_{ATF}. To further establish the specificity of compound **5**, we tested whether the compound inhibited the interaction between uPAR and 8B12,[28] a monoclonal antibody that binds to the vitronectin binding site of uPAR (SI; Figure S2). The antibody binds tightly to uPAR with a K_d of 20.6 ± 1.1 nM. BLI sensors with immobilized 8B12 were dipped into wells containing uPAR preincubated with increasing concentration of compounds **5** or **8**. Neither **5** nor **8** (IPR-3430) inhibited the interaction between uPAR and 8B12. If the compounds were aggregating the protein or nonspecifically inhibiting uPAR, we would expect inhibition in this assay. We used microscale thermophoresis (MST) to measure direct binding of compounds **5**, **8**, and **9** (IPR-3432) to uPAR (SI; Figure S3). Compound **9** showed good binding to uPAR with a K_d of 13.0 ± 3.0 μM. We did not detect binding of **5** and **8** to apo uPAR, possibly because these compounds may bind with higher affinity to uPAR when it is in complex with uPA. The binding of **9** provides evidence of direct engagement of uPAR by these compounds.

Design and Synthesis of Derivatives of 5. Another 11 derivatives (**7**−**17**) were prepared based on the scaffold of **5**, with the thiophene group on the quinoline core (Table 1). As

https://dx.doi.org/10.1021/acsmedchemlett.0c00422
ACS Med. Chem. Lett. 2021, 12, 60−66

Table 1. Derivatives of 1 (IPR-2992)

	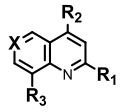						
Compound	**X**	**R_1**	**R_2**	**R_3**	**FP IC_{50} (μM) | Max (%)**	**ELISA IC_{50} (μM)**	**ALogP**
1 (IPR-2992)	C			-CH_3	89.7 ± 12.2 | 100	141 ± 19.0	3.6
2 (IPR-3238)	C				9.8 ± 1.8 | 22	13.9 ± 1.5	4.6
3 (IPR-3239)	C			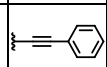	8.0 ± 8.5 | 29	50.0 ± 6.0	5.2
4 (IPR-3241)	C			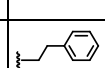	6.2 ± 2.1 | 21	NI	5.5
5 (IPR-3242)	C				4.9 ± 2.1 | 47	0.5 ± 0.0	4.3
6 (IPR-3243)	C			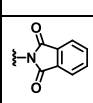	25.0 ± 5.4 | 44	73.8 ± 9.7	3.7
7 (IPR-3429)	C				7.5 ± 1.5 | 28	0.5 ± 0.1	4.5
8 (IPR-3430)	C				22.7 ± 5.8 | 100	8.5 ± 0.7	3.2
9 (IPR-3432)	N				9.3 ± 0.6 | 32	10.4 ± 0.7	3.2
10 (IPR-3469)	C		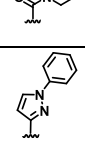		NI	NI	6.9
11 (IPR-3470)	C		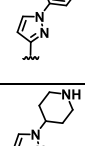		9.5 ± 0.7 | 100	NI	4.9
12 (IPR-3471)	C				NI	NI	5.1
13 (IPR-3489)	C				NI	13.4 ± 1.9	6.9
14 (IPR-3490)	C				12.0 ± 4.6 | 28	2.2 ± 0.2	4.3
15 (IPR-3491)	C				13.1 ± 0.9 | 69	NI	4.0
16 (IPR-3492)	C				12.3 ± 10.1 | 28	2.2 ± 0.2	4.3
17 (IPR-3493)	C				5.8 ± 2.7 | 17	80.5 ± 15.0	3.3

with **5**, these derivatives showed differences in the inhibition potencies detected by FP assay (Figure 4A) compared to the competition assays that involved the full protein interface like ELISA (Figure 4B) and BLI (Figure 4C). Addition of a fluorine

https://dx.doi.org/10.1021/acsmedchemlett.0c00422
ACS Med. Chem. Lett. 2021, 12, 60−66

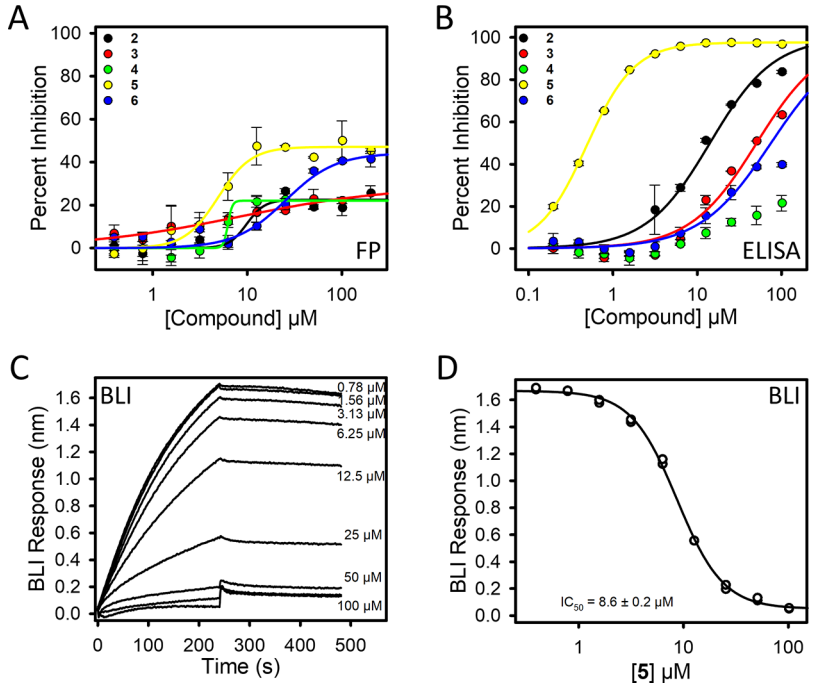

Figure 2. Derivatives of IPR-2992 inhibit uPAR binding to uPA. (A) Concentration-dependent inhibition of uPAR binding to AE147-FAM peptide in an FP assay (mean ± SD; $n = 3$). (B) Concentration-dependent inhibition of uPAR binding to uPA_{ATF} in an ELISA-based assay (mean ± SD; $n = 3$). (C) Concentration-dependent inhibition of uPAR binding to uPA_{ATF} in a biolayer interferometry (BLI) assay. Representative sample readings of 30 nM uPAR with various concentrations of **5** (IPR-3242). (D) Concentration-dependent inhibition of uPAR binding to uPA_{ATF} ($n = 2$).

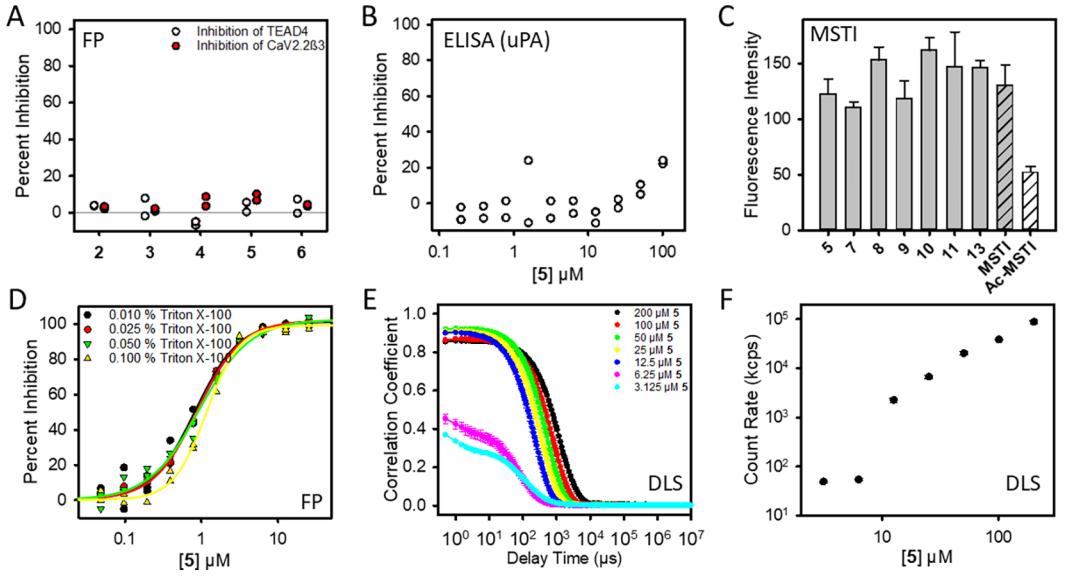

Figure 3. Compound **5** inhibits without assay interference. (A) Compounds **2**−**6** were tested against unrelated protein−protein interactions, TEAD4· and Cav2.2$_{\beta 3}$·AID at 100 μM concentration in FP-based inhibition assay ($n = 2$). (B) Compound **5** (IPR-3242) was preincubated with immobilized uPA_{ATF} in the ELISA assay to test whether the compound functioned through uPA_{ATF} or whether the compound can dislodge uPA_{ATF} from plate surface. After incubation with uPA_{ATF}, the compound was washed away and uPAR was added and detected ($n = 2$). (C) Compound **5** and its derivatives were tested for their reactivity toward cysteines by their interaction with MSTI. MSTI with DMSO is used as a no reaction control and acetyl-MSTI is used as a positive reaction control (mean ± SD; $n = 3$). (D) Concentration-dependent inhibition of uPAR binding to uPA_{ATF} in an ELISA-based inhibition assay, where the concentration of detergent Triton-X100 was increased to prevent aggregation in samples ($n = 2$). (E) Concentration-dependent DLS analysis of **5** in PBS with 0.01% Triton X-100. Correlogram shows detection of particles at concentrations higher than 12.5 μM (mean ± SD; $n = 3$). (F) Concentration-dependent DLS analysis of **5** in PBS with 0.01% Triton X-100. The count rate expressed in kilocounts per second (kcps) increased with concentration indicating aggregation at concentrations greater than 12.5 μM (mean ± SD; $n = 3$).

at the *meta*-position of the phenyl moiety of **5** as in compound **7** (IPR-3429) did not have an effect on ELISA IC_{50}. However, methoxy at the *meta*- and *para*-positions such as in **14** (IPR-3490) and **16** (IPR-3492), respectively, increased the ELISA IC_{50}'s by 4.4-fold (Table 1). Replacing the benzene ring of **5** with pyridine in **8** further weakened the compound by 17-fold to an IC_{50} of 8.5 ± 0.7 μM. Addition of a nitrogen into the quinoline core to produce naphthyridine **9** led to similar loss in

https://dx.doi.org/10.1021/acsmedchemlett.0c00422
ACS Med. Chem. Lett. 2021, 12, 60−66

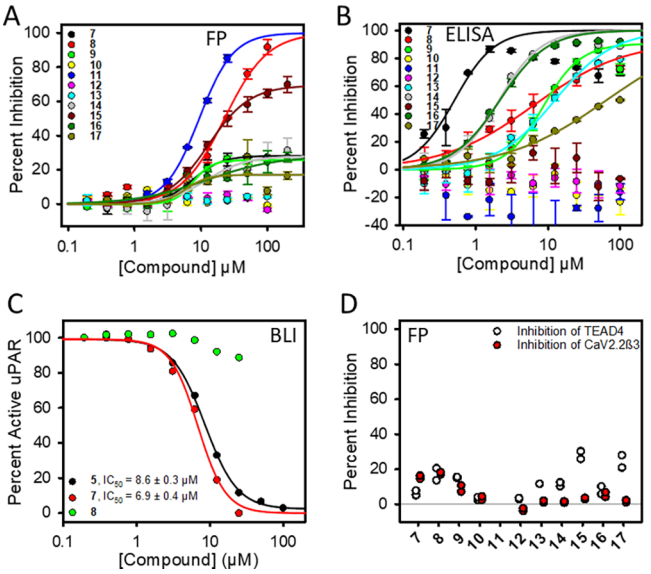

Figure 4. Derivatives of **5** inhibit uPAR binding to uPA. (A) Concentration-dependent inhibition of uPAR binding to AE147-FAM peptide in FP assay (mean ± SD; n = 3). (B) Concentration-dependent inhibition of uPAR binding to uPA_{ATF} in an ELISA-based assay (mean ± SD; n = 3). (C) Concentration-dependent inhibition of uPAR binding to uPA_{ATF} (BLI) by select compounds (n = 1). (D) Compounds **7**−**17** were tested against unrelated protein−protein interactions, TEAD4·and Cav2.2$_{\beta 3}$·AID, at 100 μM concentration in FP-based inhibition assay (n = 2).

potency resulting in IC_{50} of 10.4 ± 0.7 μM. Changing the morpholine ring to a piperazine in **15** (IPR-3491) led to complete loss of inhibition. However, extending it further in **13** (IPR-3489) led to some inhibition with an IC_{50} of 13.4 ± 1.9 μM, which is still 27-fold weaker than **5**. Other changes were more dramatic such as the replacement of the morpholinomethanone at position 4 on the quinolone ring with a diazole as in **12** (IPR-3471) led to complete loss of inhibition. Addition of a benzene ring to the diazole such as in **13** (IPR-3489) and **14** led to compounds that inhibited with IC_{50}s in the double-digit micromolar range. Finally, modification of the thiophene to a thiazole as in **17** (IPR-3493) led to 160-fold loss in IC_{50} to 80.5 ± 15.0 μM.

To confirm the inhibition that we observed by ELISA, compounds **7** and **8** were tested on a separate BLI assay (Figure 4C). Consistent with the ELISA, compound **7** had similar IC_{50} to **5**, while **8** did not inhibit well, which is consistent with the 21-fold increase in IC_{50} observed in the ELISA for this compound. Like compound **5**, **7**−**17** did not inhibit unrelated PPIs such as TEAD4·and Cav2.2$_{\beta 3}$·AID (Figure 4D). Furthermore, as with **5**, the derivatives were not cysteine-reactive in the MSTI assay (Figure 3C).

In a previous study, we identified fragment-like compound **1**.[25] Here, as we explored the role of additional substituents on the quinolone ring of **1**, we discovered **5**. The compound exhibited potent inhibition of the uPAR·uPA interaction using ELISA and BLI competition assays. The IC_{50} in the ELISA was submicromolar and single-digit micromolar using BLI. The high inhibition potency, which we have rarely seen for a small molecule, especially a sub-500 Da molecular weight compound, prompted us to explore whether the inhibition was due to artifacts, such as possible lack of stability and covalent reaction, or by aggregation. MSTI assay ruled out covalent bond formation. Repeating the ELISA with 10-fold higher levels of Triton-X100 showed no effect on the inhibition profile of the compound, which suggested that aggregation is likely not the mechanism of inhibition. It is worth noting that at higher concentrations, namely 12.5 μM or higher, dynamic light scattering did detect potential aggregation. Inhibition curves of the compounds do not support an aggregation mechanism, which usually exhibits sharp increases in activity over a small concentration range.[29] We tested whether the compound inhibited the binding of an antibody (8B12) to the vitronectin binding site of uPAR, which is distinct from the uPA-binding site. The compound did not inhibit this high-affinity interaction, suggesting that it is specific to the uPAR·uPA interaction.

Compound **5**, as well as several derivatives, inhibited the binding of fluorescently labeled AE-147 peptide to uPAR. The peptide, AE147, was shown by X-ray crystallography to bind to the central pocket of uPAR occupied by the β-hairpin of the ATF domain of uPAR.[15] It was surprising that the compound did not completely inhibit binding of AE147 to uPAR even at higher concentrations. The FP data for **5** and derivatives supports the fact that the compound may be binding directly but plateauing of the curve to values below 100% suggests that the compounds are not directly competing with the fluorescent peptide.

Collectively, the FP, BLI, and ELISA data for **5** and derivatives suggest that the compounds possibly bind outside of the uPAR·uPA interface and trap uPAR into a conformation that is not capable of engaging uPA. This inhibition mechanism is likely uPAR-specific since it was not detected with other protein−protein interactions. For example, when the compound is tested for inhibition of the TEAD·Yap1 and CaV2.2$_{\beta 3}$·AID interactions, we found no inhibition. Both of these interactions are high affinity and occur over a large interface. Additional studies will be required to determine the solution structures of uPAR that bind to the compounds. Further studies will have to be performed to determine whether this inhibition mechanism can occur at the cell surface.

■ ASSOCIATED CONTENT

Supporting Information

The Supporting Information is available free of charge at https://pubs.acs.org/doi/10.1021/acsmedchemlett.0c00422.

Materials and Methods describing protein expression and purification, fluorescence polarization assay, ELISA, biolayer interferometry, microscale thermophoresis, and dynamic light scattering assays; synthesis and characterization of all compounds (PDF)

■ AUTHOR INFORMATION

Corresponding Author

Samy O. Meroueh − *Department of Biochemistry and Molecular Biology, Indiana University School of Medicine, Indianapolis, Indiana 46202, United States;* orcid.org/0000-0002-3948-7499; Phone: (317) 274-8315; Email: smeroueh@iu.edu; Fax: (317) 278-9217

Authors

Khuchtumur Bum-Erdene − *Department of Biochemistry and Molecular Biology, Indiana University School of Medicine, Indianapolis, Indiana 46202, United States*

Degang Liu − *Department of Biochemistry and Molecular Biology, Indiana University School of Medicine, Indianapolis, Indiana 46202, United States*

https://dx.doi.org/10.1021/acsmedchemlett.0c00422
ACS Med. Chem. Lett. 2021, 12, 60−66

David Xu − *Center for Computational Biology and Bioinformatics, Indiana University School of Medicine, Indianapolis, Indiana 46202, United States;* orcid.org/0000-0003-3949-0599

Mona K. Ghozayel − *Department of Biochemistry and Molecular Biology, Indiana University School of Medicine, Indianapolis, Indiana 46202, United States*

Complete contact information is available at: https://pubs.acs.org/10.1021/acsmedchemlett.0c00422

Notes

The authors declare no competing financial interest.

■ ACKNOWLEDGMENTS

The research was supported by the National Institutes of Health (R01CA197928) (SOM), the American Cancer Society Research Scholar Grant RSG-12-092-01-CDD (SOM), and the 100 Voices of Hope (SOM).

■ REFERENCES

(1) Magdolen, V.; Rettenberger, P.; Koppitz, M.; Goretzkt, L.; Kessler, H.; Weidle, U. H.; Konig, B.; Graeff, H.; Schmitt, M.; Wilhelm, O. Systematic mutational analysis of the receptor-binding region of the human urokinase-type plasminogen activator. *Eur. J. Biochem.* **1996**, *237* (3), 743−51.

(2) Gardsvoll, H.; Ploug, M. Mapping of the vitronectin-binding site on the urokinase receptor: involvement of a coherent receptor interface consisting of residues from both domain I and the flanking interdomain linker region. *J. Biol. Chem.* **2007**, *282* (18), 13561−72.

(3) Madsen, C. D.; Ferraris, G. M.; Andolfo, A.; Cunningham, O.; Sidenius, N. uPAR-induced cell adhesion and migration: vitronectin provides the key. *J. Cell Biol.* **2007**, *177* (5), 927−39.

(4) Huai, Q.; Zhou, A.; Lin, L.; Mazar, A. P.; Parry, G. C.; Callahan, J.; Shaw, D. E.; Furie, B.; Furie, B. C.; Huang, M. Crystal structures of two human vitronectin, urokinase and urokinase receptor complexes. *Nat. Struct. Mol. Biol.* **2008**, *15* (4), 422−423.

(5) Crowley, C. W.; Cohen, R. L.; Lucas, B. K.; Liu, G. H.; Shuman, M. A.; Levinson, A. D. Prevention of Metastasis by Inhibition of the Urokinase Receptor. *Proc. Natl. Acad. Sci. U. S. A.* **1993**, *90* (11), 5021−5025.

(6) Ignar, D. M.; Andrews, J. L.; Witherspoon, S. M.; Leray, J. D.; Clay, W. C.; Kilpatrick, K.; Onori, J.; Kost, T.; Emerson, D. L. Inhibition of establishment of primary and micrometastatic tumors by a urokinase plasminogen activator receptor antagonist. *Clin. Exp. Metastasis* **1997**, *16* (1), 9−20.

(7) Kobayashi, H.; Sugino, D.; She, M. Y.; Ohi, H.; Hirashima, Y.; Shinohara, H.; Fujie, M.; Shibata, K.; Terao, T. A bifunctional hybrid molecule of the amino-terminal fragment of urokinase and domain II of bikunin efficiently inhibits tumor cell invasion and metastasis. *Eur. J. Biochem.* **1998**, *253* (3), 817−826.

(8) Wei, Y.; Lukashev, M.; Simon, D. I.; Bodary, S. C.; Rosenberg, S.; Doyle, M. V.; Chapman, H. A. Regulation of integrin function by the urokinase receptor. *Science* **1996**, *273* (5281), 1551−1555.

(9) Wei, Y.; Eble, J. A.; Wang, Z. M.; Kreidberg, J. A.; Chapman, H. A. Urokinase receptors promote beta 1 integrin function through interactions with integrin alpha 3 beta 1. *Mol. Biol. Cell* **2001**, *12* (10), 2975−2986.

(10) Berkenblit, A.; Matulonis, U. A.; Kroener, J. F.; Dezube, B. J.; Lam, G. N.; Cuasay, L. C.; Brunner, N.; Jones, T. R.; Silverman, M. H.; Gold, M. A. A6, a urokinase plasminogen activator (uPA)-derived peptide in patients with advanced gynecologic cancer: a phase I trial. *Gynecol. Oncol.* **2005**, *99* (1), 50−7.

(11) Guo, Y.; Higazi, A. A.; Arakelian, A.; Sachais, B. S.; Cines, D.; Goldfarb, R. H.; Jones, T. R.; Kwaan, H.; Mazar, A. P.; Rabbani, S. A. A peptide derived from the nonreceptor binding region of urokinase plasminogen activator (uPA) inhibits tumor progression and angiogenesis and induces tumor cell death in vivo. *FASEB J.* **2000**, *14* (10), 1400−10.

(12) Lin, L.; Gardsvoll, H.; Huai, Q.; Huang, M.; Ploug, M. Structure-based engineering of species selectivity in the interaction between urokinase and its receptor: implication for preclinical cancer therapy. *J. Biol. Chem.* **2010**, *285* (14), 10982−92.

(13) Gardsvoll, H.; Dano, K.; Ploug, M. Mapping part of the functional epitope for ligand binding on the receptor for urokinase-type plasminogen activator by site-directed mutagenesis. *J. Biol. Chem.* **1999**, *274* (53), 37995−8003.

(14) Huai, Q.; Mazar, A. P.; Kuo, A.; Parry, G. C.; Shaw, D. E.; Callahan, J.; Li, Y.; Yuan, C.; Bian, C.; Chen, L. Structure of human urokinase plasminogen activator in complex with its receptor. *Science* **2006**, *311* (5761), 656.

(15) Llinas, P.; Le Du, M. H.; Gardsvoll, H.; Dano, K.; Ploug, M.; Gilquin, B.; Stura, E. A.; Menez, A. Crystal structure of the human urokinase plasminogen activator receptor bound to an antagonist peptide. *EMBO J.* **2005**, *24* (9), 1655−63.

(16) Gardsvoll, H.; Gilquin, B.; Le Du, M. H.; Menez, A.; Jorgensen, T. J.; Ploug, M. Characterization of the functional epitope on the urokinase receptor. Complete alanine scanning mutagenesis supplemented by chemical cross-linking. *J. Biol. Chem.* **2006**, *281* (28), 19260−72.

(17) Mani, T.; Liu, D.; Zhou, D.; Li, L.; Knabe, W. E.; Wang, F.; Oh, K.; Meroueh, S. O. Probing binding and cellular activity of pyrrolidinone and piperidinone small molecules targeting the urokinase receptor. *ChemMedChem* **2013**, *8* (12), 1963−77.

(18) Mani, T.; Wang, F.; Knabe, W. E.; Sinn, A. L.; Khanna, M.; Jo, I.; Sandusky, G. E.; Sledge, G. W., Jr.; Jones, D. R.; Khanna, R.; Pollok, K. E.; Meroueh, S. O. Small-molecule inhibition of the uPAR.uPA interaction: synthesis, biochemical, cellular, in vivo pharmacokinetics and efficacy studies in breast cancer metastasis. *Bioorg. Med. Chem.* **2013**, *21* (7), 2145−55.

(19) Wang, F.; Eric Knabe, W.; Li, L.; Jo, I.; Mani, T.; Roehm, H.; Oh, K.; Li, J.; Khanna, M.; Meroueh, S. O. Design, synthesis, biochemical studies, cellular characterization, and structure-based computational studies of small molecules targeting the urokinase receptor. *Bioorg. Med. Chem.* **2012**, *20* (15), 4760−73.

(20) Liu, D.; Zhou, D.; Wang, B.; Knabe, W. E.; Meroueh, S. O. A New Class of Orthosteric uPAR.uPA Small-Molecule Antagonists Are Allosteric Inhibitors of the uPAR. Vitronectin Interaction. *ACS Chem. Biol.* **2015**, *10* (6), 1521−34.

(21) Khanna, M.; Wang, F.; Jo, I.; Knabe, W. E.; Wilson, S. M.; Li, L.; Bum-Erdene, K.; Li, J.; G, W. S.; Khanna, R.; Meroueh, S. O. Targeting multiple conformations leads to small molecule inhibitors of the uPAR.uPA protein-protein interaction that block cancer cell invasion. *ACS Chem. Biol.* **2011**, *6* (11), 1232−43.

(22) Rullo, A. F.; Fitzgerald, K. J.; Muthusamy, V.; Liu, M.; Yuan, C.; Huang, M.; Kim, M.; Cho, A. E.; Spiegel, D. A. Re-engineering the Immune Response to Metastatic Cancer: Antibody-Recruiting Small Molecules Targeting the Urokinase Receptor. *Angew. Chem., Int. Ed.* **2016**, *55* (11), 3642−6.

(23) Liu, M.; Lin, L.; Hoyer-Hansen, G.; Ploug, M.; Li, H.; Jiang, L.; Yuan, C.; Li, J.; Huang, M. Crystal structure of the unoccupied murine urokinase-type plasminogen activator receptor (uPAR) reveals a tightly packed DII-DIII unit. *FEBS Lett.* **2019**, *593* (11), 1236−1247.

(24) Mertens, H. D.; Kjaergaard, M.; Mysling, S.; Gardsvoll, H.; Jorgensen, T. J.; Svergun, D. I.; Ploug, M. A flexible multidomain structure drives the function of the urokinase-type plasminogen activator receptor (uPAR). *J. Biol. Chem.* **2012**, *287* (41), 34304−15.

(25) Xu, D.; Bum-Erdene, K.; Si, Y.; Zhou, D.; Ghozayel, M. K.; Meroueh, S. O. Mimicking Intermolecular Interactions of Tight Protein-Protein Complexes for Small-Molecule Antagonists. *ChemMedChem* **2017**, *12* (21), 1794−1809.

(26) Bum-Erdene, K.; Zhou, D.; Gonzalez-Gutierrez, G.; Ghozayel, M. K.; Si, Y.; Xu, D.; Shannon, H. E.; Bailey, B. J.; Corson, T. W.; Pollok, K. E.; Wells, C. D.; Meroueh, S. O. Small-Molecule Covalent Modification of Conserved Cysteine Leads to Allosteric Inhibition of

the TEADYap Protein-Protein Interaction. *Cell Chem. Biol.* **2019**, *26* (3), 378−389.
(27) Chen, X.; Liu, D.; Zhou, D.; Si, Y.; Xu, D.; Stamatkin, C. W.; Ghozayel, M. K.; Ripsch, M. S.; Obukhov, A. G.; White, F. A.; Meroueh, S. O. Small-molecule CaValpha1CaVbeta antagonist suppresses neuronal voltage-gated calcium-channel trafficking. *Proc. Natl. Acad. Sci. U. S. A.* **2018**, *115* (45), E10566−E10575.
(28) Zhao, B.; Gandhi, S.; Yuan, C.; Luo, Z.; Li, R.; Gårdsvoll, H.; de Lorenzi, V.; Sidenius, N.; Huang, M.; Ploug, M. Stabilizing a Flexible Interdomain Hinge Region Harboring the SMB Binding Site Drives uPAR into Its Closed Conformation. *J. Mol. Biol.* **2015**, *427* (6), 1389−1403.
(29) Irwin, J. J.; Duan, D.; Torosyan, H.; Doak, A. K.; Ziebart, K. T.; Sterling, T.; Tumanian, G.; Shoichet, B. K. An Aggregation Advisor for Ligand Discovery. *J. Med. Chem.* **2015**, *58* (17), 7076−7087.

https://dx.doi.org/10.1021/acsmedchemlett.0c00422
ACS Med. Chem. Lett. 2021, 12, 60−66